Electronic Supplementary Material (ESI) for Polymer Chemistry.

Cooperative Supramolecular Polymerization of Phosphorescent Alkynyl-Gold(I)–Isocyanide Complexes

*Cong Wang, Ze Chen, Mingyang Liu, Hua Zhong, and Feng Wang**

CAS Key Laboratory of Soft Matter Chemistry,
iChEM (Collaborative Innovation Center of Chemistry for Energy Materials),
Department of Polymer Science and Engineering,
University of Science and Technology of China,
Hefei, Anhui 230026 (P. R. China)
E-mail: drfwang@ustc.edu.cn.

Supporting Information

*1. Absorption and emission spectroscopy of **2a–b***

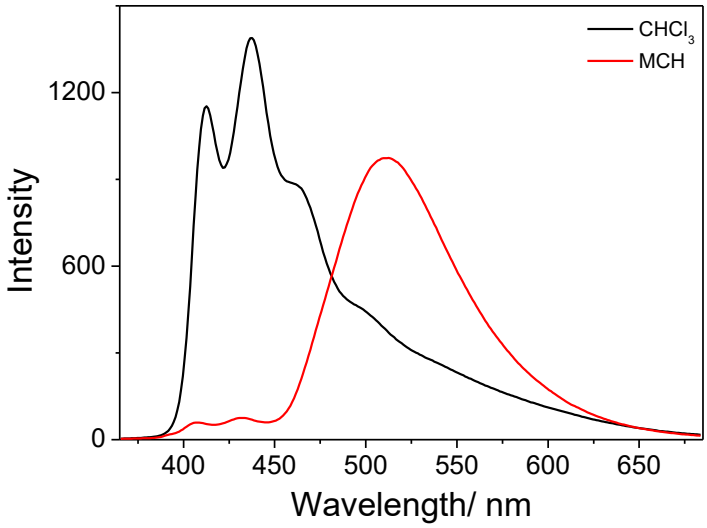

Figure S1. Emission spectra of **2b** (λ_{ex} = 350 nm**)** in $CHCl_3$ (black line) and MCH (red line).

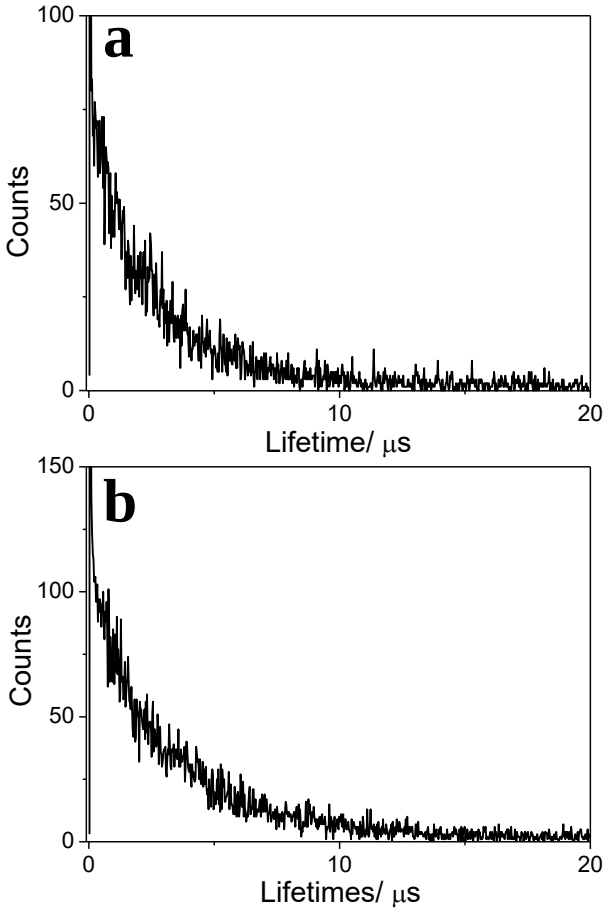

Figure S2. Lifetime measurement of a) **2a** and b) **2b** (2.00×10^{-5} M in MCH, λ_{ex} = 350 nm). The lifetime is determined to be 2.94 μs for **2a** and 3.08 μs for **2b**, suggesting the triplet origin for the emission bands.

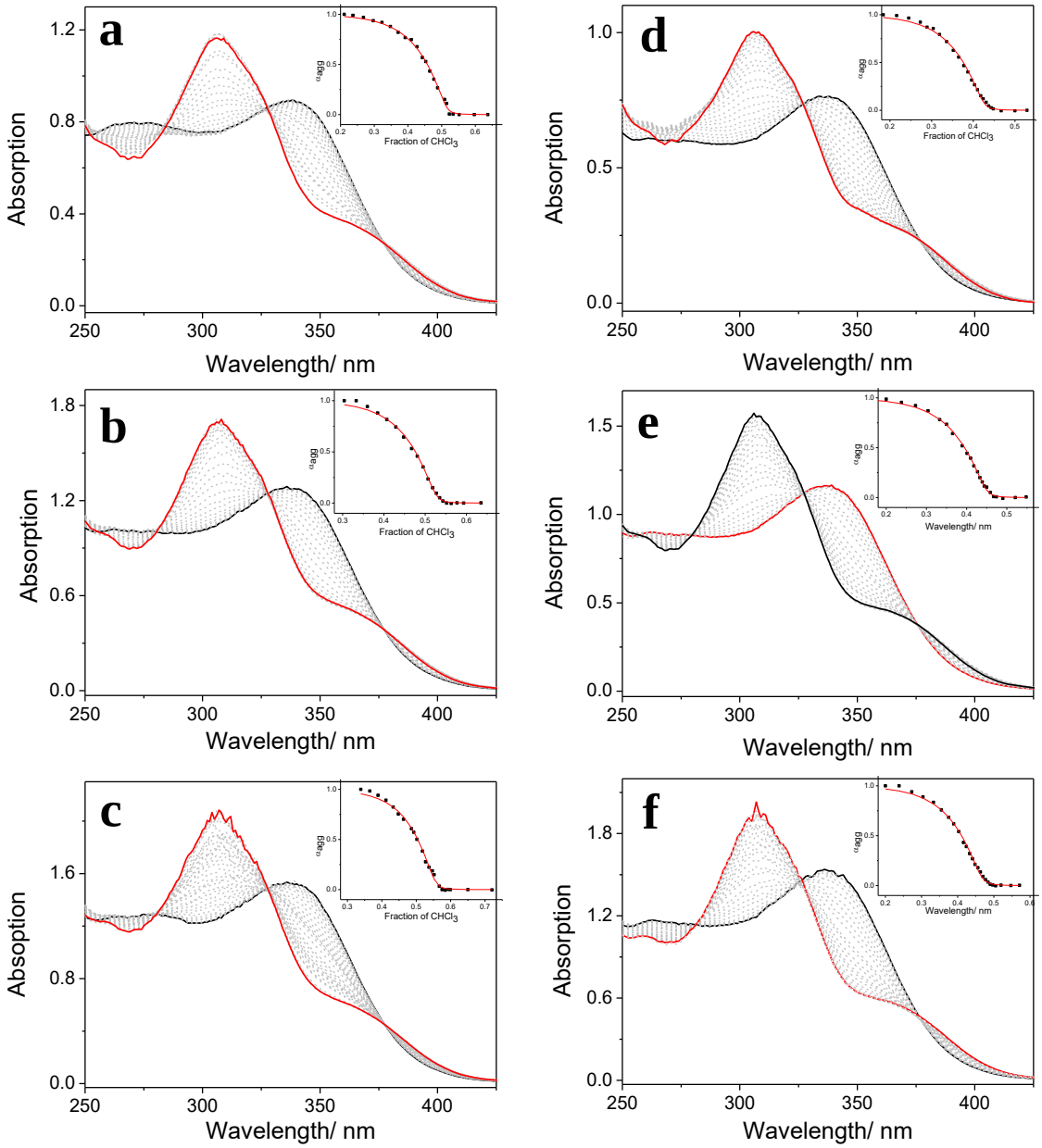

Figure S3. Solvent-dependent UV–Vis spectra (293K) of **2a–b** in MCH at different monomer concentration: a) 1.00×10^{-5} M of **2a**; b) 1.50×10^{-5} M of **2a**; c) 2.00×10^{-5} M of **2a**; d) 1.00×10^{-5} M of **2b**; e) 1.50×10^{-5} M of **2b**; f) 2.00×10^{-5} M of **2b**. Inset: normalized absorbance intensity at 348 nm *versus* $CHCl_3$ volume, and the corresponding mathematical fitting curves. The quantitative thermodynamic values are shown in Table S1.

2. CD spectroscopy of ***2b***

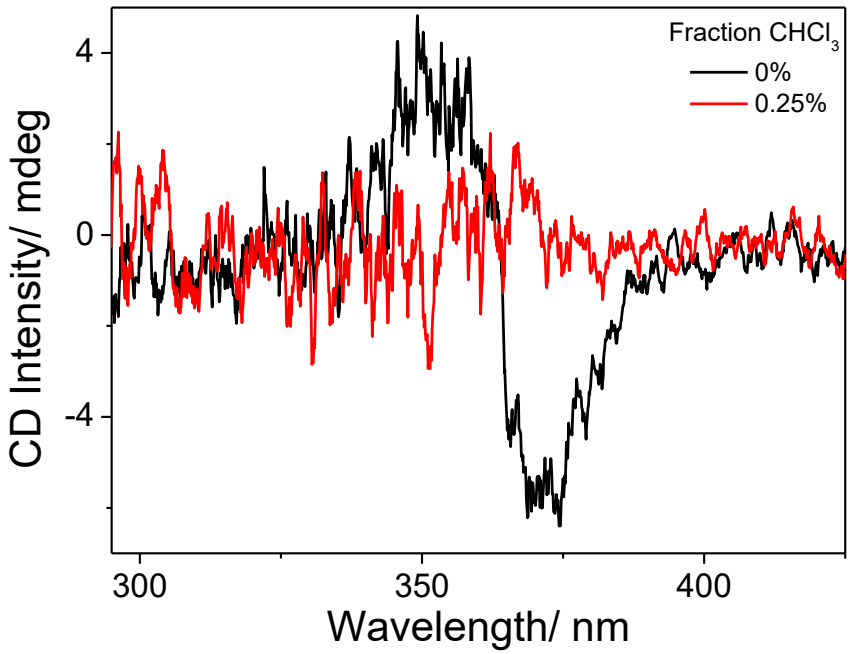

Figure S4. CD spectra of **1a** (c = 2.00 × 10^{-4} M, 273 K, 1 mm cuvette) at different fraction of $CHCl_3$: 0.00% (black line) and 0.25% (red line). As can be seen, the CD signal disappears upon adding trace amount of $CHCl_3$.

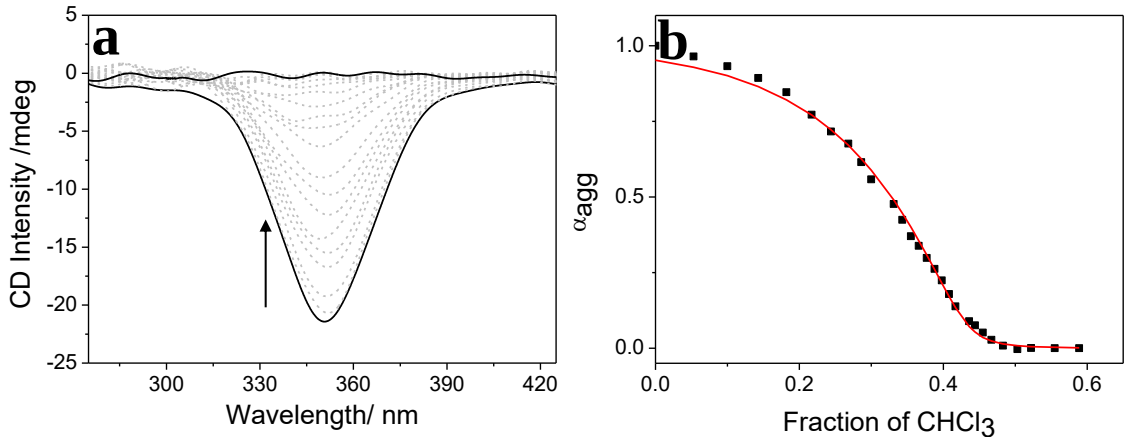

Figure S5. a) Solvent-dependent CD spectra of **2b** (c = 1.50 × 10^{-5} M in MCH, 293K, 10 mm cuvette). b) Normalized CD intensity of **2b** at 348 nm *versus* $CHCl_3$ volume fraction (from 0.00 to 0.59). The critical chloroform volume fraction (46.0%) is consistent with that acquired from UV–Vis experiments under the same conditions (46.2%).

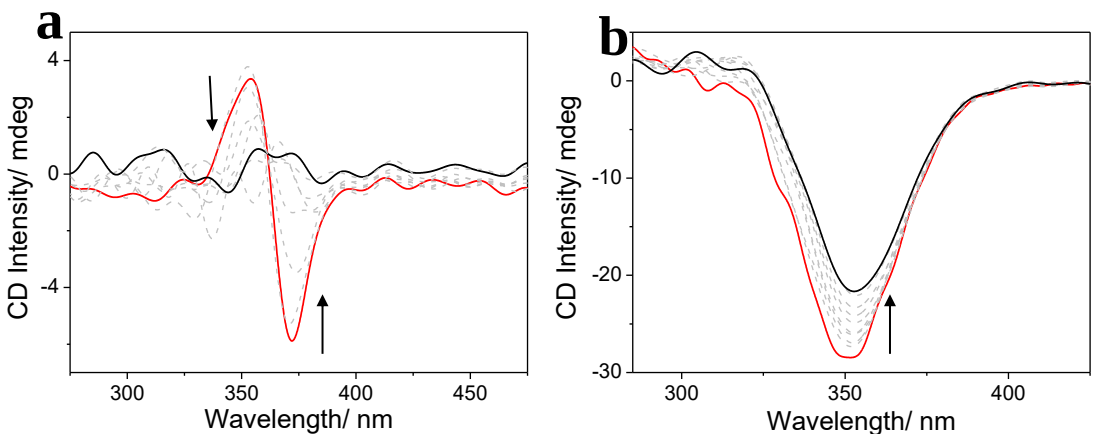

Figure S6. a) Solvent-dependent CD spectra of a) **1a**; and b) **2b** (2.00×10^{-4} M in MCH, 1 mm cuvette). Arrows indicate the spectral changes upon increasing toluene fraction (a: from 0% to 8%, and b: from 0% to 100%) The CD signal for **1a** disappears upon adding small amount of toluene, suggesting the complete breakup of supramolecular polymeric structure. On the contrary, the CD signals for **2b** maintain even in pure toluene, reflecting the sufficient stability of the self-assembled helical structure.

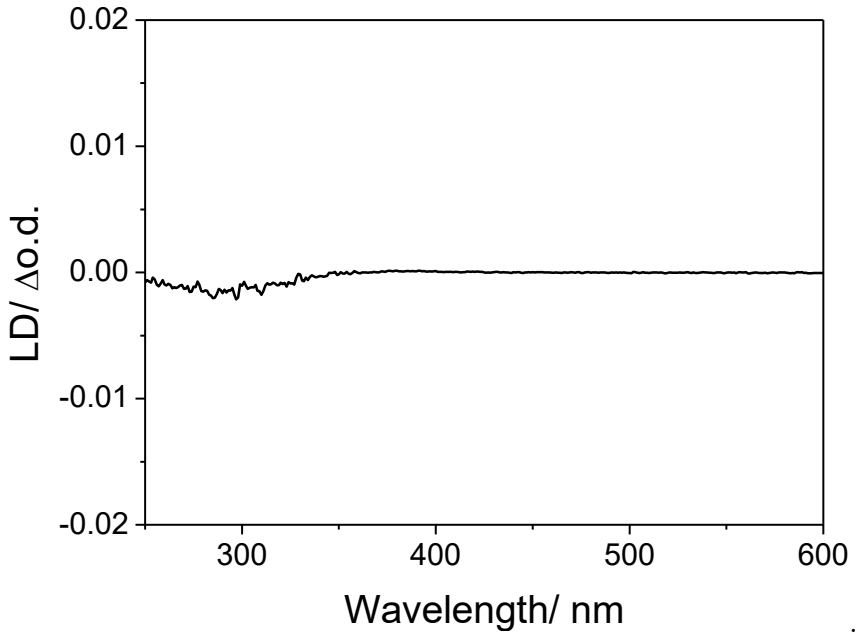

Figure S7. LD spectrum of **2a** (1.50×10^{-5} M in MCH, 293K). As can be seen, no LD signal is detected for the CD-active samples, demonstrating the measured CD signals are real to reflect the supramolecular chirality.

3. *^{1}H NMR measurements of **2a–b***

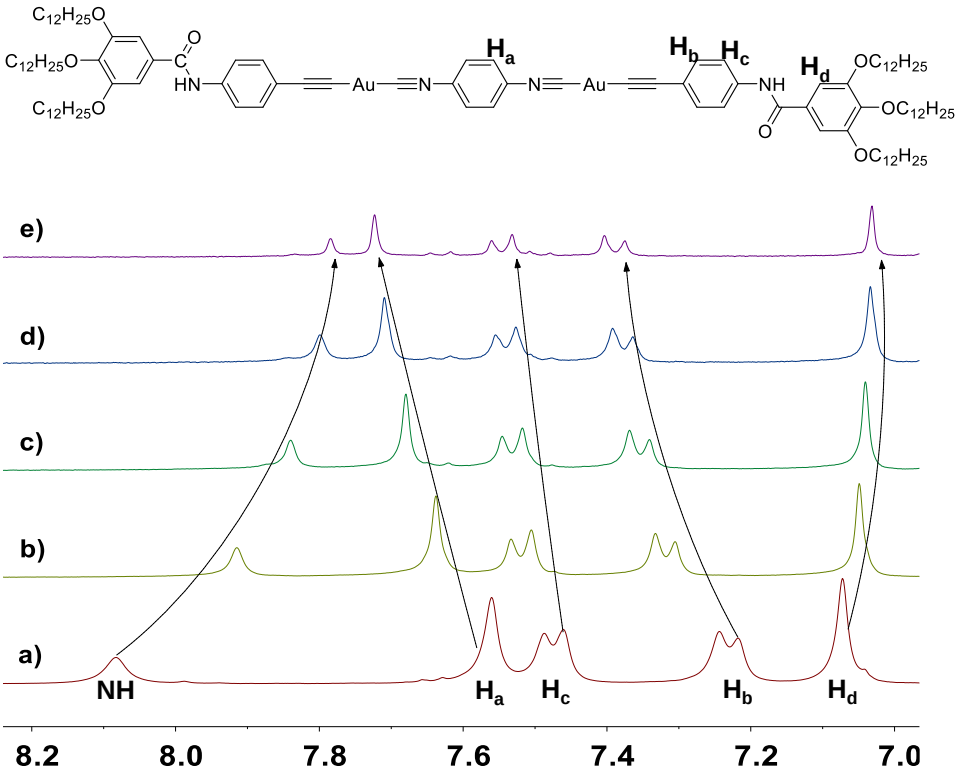

Figure S8. Concentration-dependent ^{1}H NMR spectra (400 MHz, CD_2Cl_2, 298 K) of **2a**: a) 20.0 mM; b) 10.0 mM; c) 5.00 mM; d) 2.50 mM; e) 1.25 mM. Upon increasing the monomer concentration from 0.26 to 20 mM, the amide N–*H* protons undergo significant downfield shifts from 7.78 to 8.08 ppm ($\Delta\delta$: –0.30 ppm), while the aromatic protons on **2a** shift upfield ($\Delta\delta$: 0.16, 0.15, and 0.07 ppm for H_a, H_b, and H_c, respectively). The phenomena illustrate the prominent roles of both hydrogen bonding and π–π stacking interactions for intermolecular aggregation process.

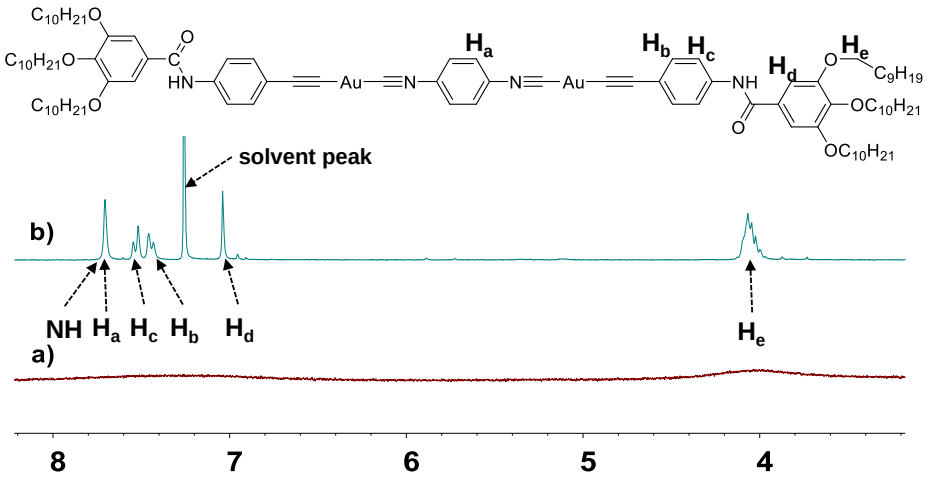

Figure S9. Partial ^{1}H NMR spectra of **2b** in a) d_{12}-cyclohexane and b) *d*-chloroform at 2.00 mM. **2b** shows broadened and indiscernible signals, indicative of the formation of high-molecular-weight polymeric structure.

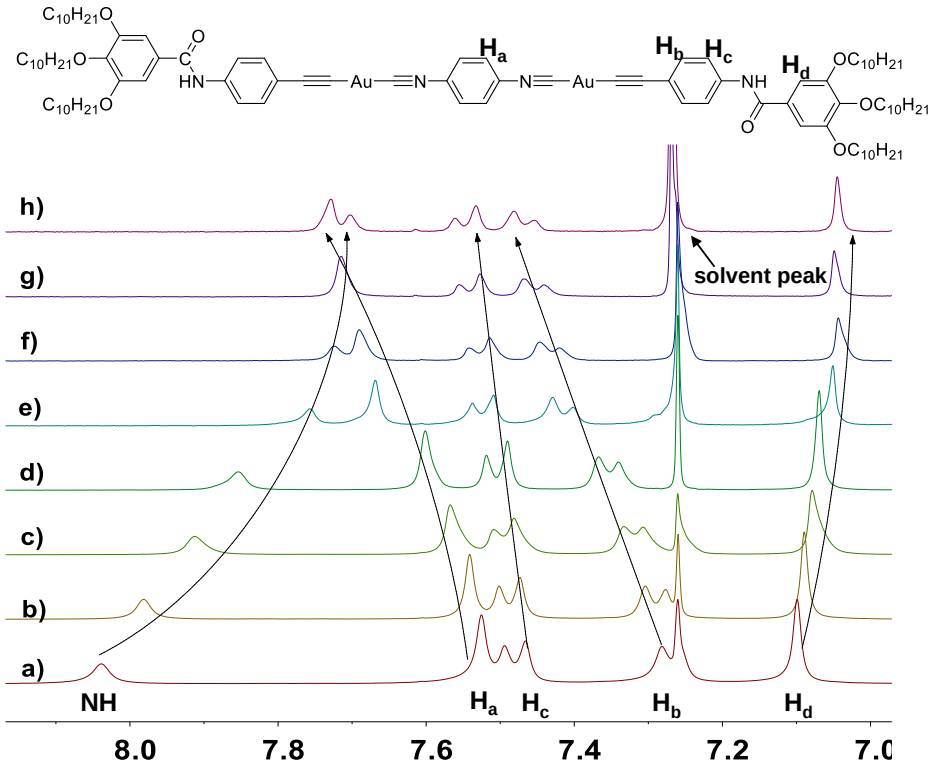

Figure S10. Concentration-dependent ^{1}H NMR spectra (400 MHz, $CDCl_3$, 298 K) of **2b**: a) 20.0 mM; b) 16.0 mM; c) 11.4 mM; d) 8.00 mM; e) 4.00 mM; f) 2.67 mM; g) 2.00 mM; h) 1.25 mM. Upon increasing the monomer concentration from 1.25 to 20 mM, the amide N–*H* protons undergo significant downfield shifts from 7.70 to 8.04 ppm ($\Delta\delta$: –0.34 ppm), while the aromatic protons on **2b** shift upfield ($\Delta\delta$: 0.19, 0.19, and 0.06 ppm for H_a, H_b, and H_c, respectively). The phenomena illustrate the prominent roles of both hydrogen bonding and π–π stacking interactions for intermolecular aggregation process.

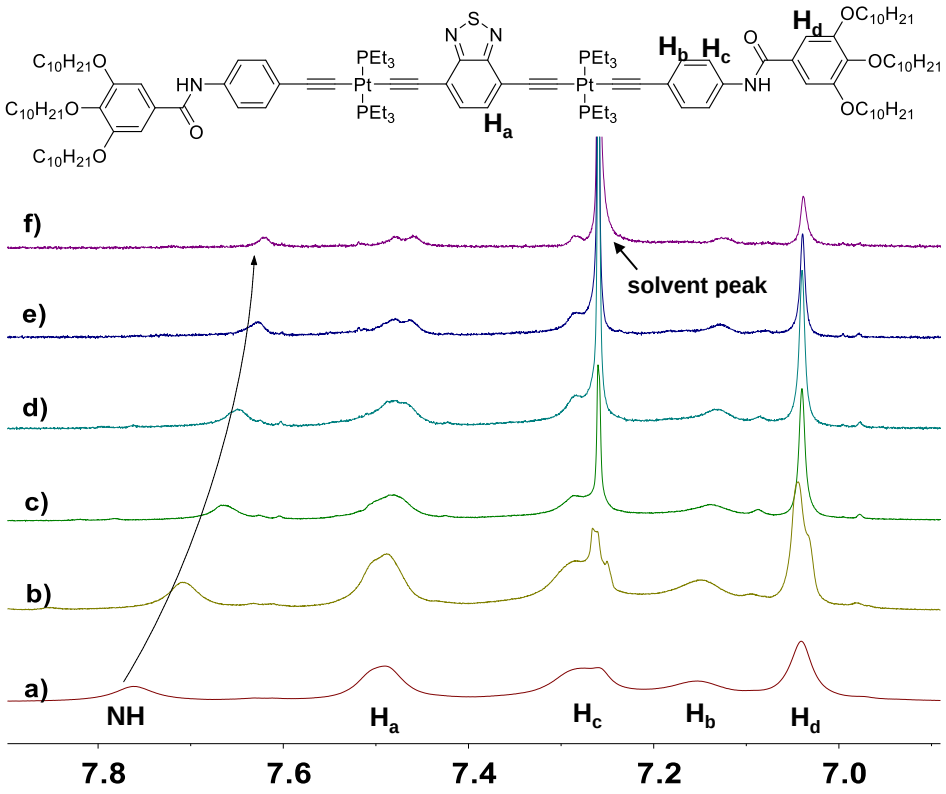

Figure S11. Concentration-dependent ^{1}H NMR spectra (400 MHz, $CDCl_3$, 298 K) of **1a**: a) 40.0 mM; b) 20.0 mM; c) 10.0 mM; d) 5.00 mM; e) 2.50 mM; f) 1.25 mM. No aromatic signal changes occur for **1a**, while the amide N–H resonances exhibit slight downfield shift (from 7.62 to 7.71 ppm, $\Delta\delta$: –0.09 ppm). It suggests that only hydrogen bonds play critical role, while π–π stacking is absent for the **1a** self-assembly process.

*4. Macroscopic gelation behaviors of **2a–b***

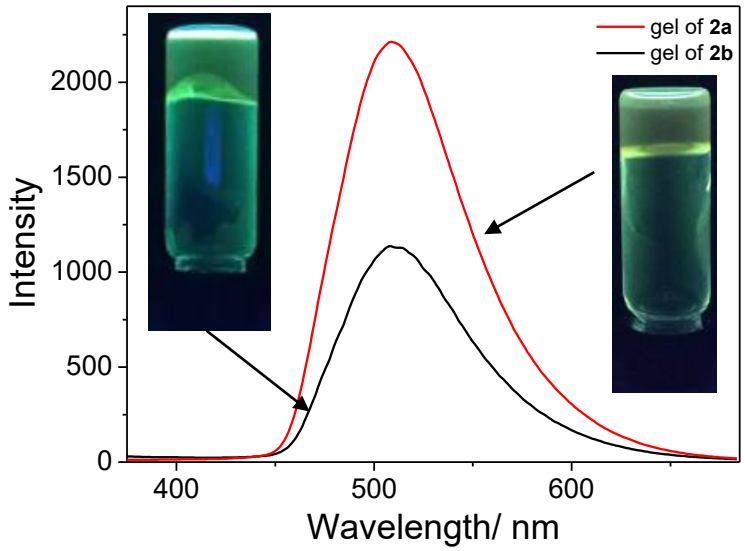

Figure S12. Emission spectra of **2a** (red line) and **2b** (black line) in the gel state (10.0 mM in MCH/$CHCl_3$, 95 : 5 (*v*/*v*), λ_{ex} = 350 nm). Inset pictures: gels under 365 nm UV lamp.

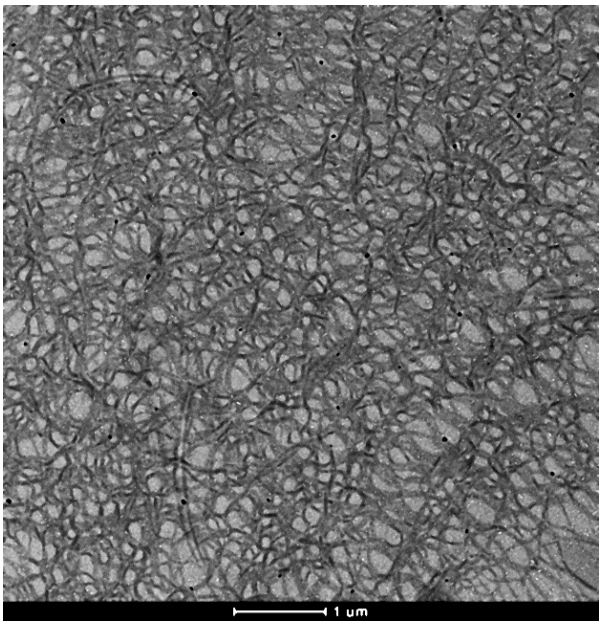

Figure S13. TEM image of **2b** (copper grid, drop-casting from 0.40 mM solution in MCH/$CHCl_3$(95 : 5, *v*/*v*)). One-dimensional fibres are observed for **2b**, laying the basis for the formation of three-dimensional supramolecular gels.

*5. Light-harvesting behavior of **2b**/**1b***

Determination of fluorescence resonance energy transfer (FRET) efficiency: spectral overlap integral $J(\lambda)$ between the emission spectra of donor and absorption spectra of acceptor is calculated according to Eq. S2:

$$J(\lambda) = \int_0^\infty f_D(\lambda)\varepsilon_A(\lambda)\lambda^4 d\lambda \qquad \textbf{(Eq. S1)}$$

In this equation, λ and $\varepsilon_A(\lambda)$ are the wavelength (cm) and molar extinction coefficient of FRET acceptor (**1b**) at the selected wavelength, respectively. $f_D(\lambda)$ is the fraction of fluorescent intensity of FRET donor (**2b**). The spectra overlap between the emission spectrum of **2b** and the extinction spectrum of **1b** is shown in Figure 5a in the main text. The overlap integral $J(\lambda)$ is calculated to be 1.99×10^{12} M^{-1} cm^{-1} nm^3.

FRET efficiency (Φ_{ET}) is calculated according to Eq. S3:[S1]

$$\phi_{ET} = 1 - I_{DA}/I_D \qquad \textbf{(Eq. S2)}$$

In this equation, I_{DA} and I_D are the emission intensities of FRET donor with and without the presence of FRET acceptor, respectively.

Energy transfer rate constant (K_{ET}) is calculated according to Eq. S4:[S2]

$$\phi_{ET} = K_{ET}/(K_{ET} + \tau_D^{-1}) \qquad \textbf{(Eq. S3)}$$

In this equation, τ_D is the emission lifetime of donor **2b** in MCH.

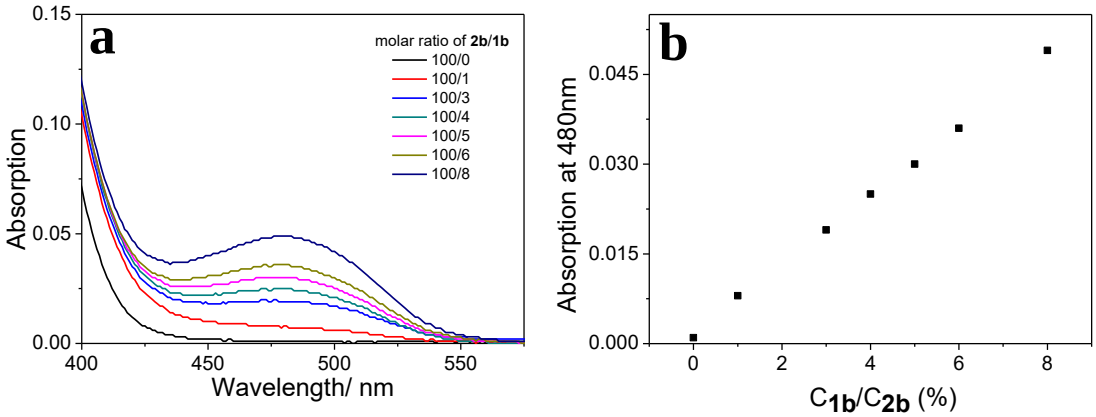

Figure S14. a) UV–Vis spectra of **2b** with the presence of different amount of **1b**. b) Absorbance at 480 nm displays the linear relationship upon increasing the amount of **1b**. The result suggests the absence of ground-state interaction between the antenna (**2b**) and acceptor (**1b**) units.

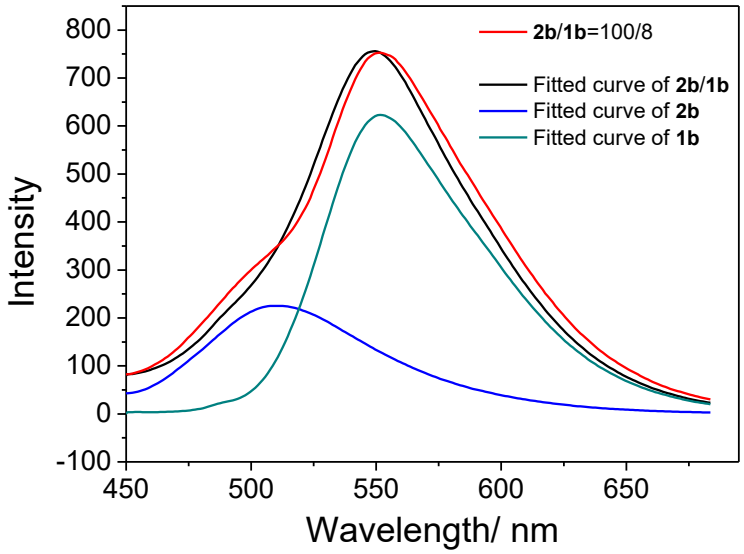

Figure S15. Peak-differentiation-imitating spectra of the emission spectra of **2b**/**1b**. Herein **2b**/**1b** = 100 : 8 is taken as an example. The quantitative energy-transfer efficiency (Φ_{ET}) is calculated to 69.0%.

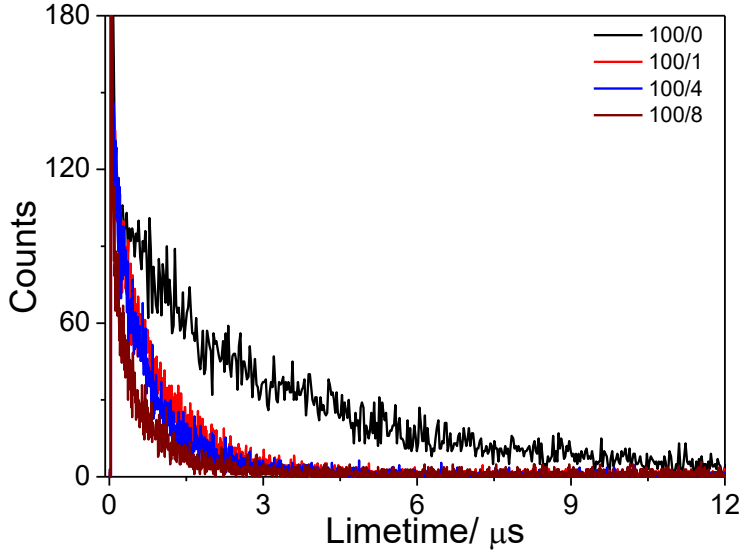

Figure S16. Lifetime decay of **2b** with the presence of different amount of **1b**. Upon varying the molar ratio of **2b**/**1b** from 100 : 0 to 100 : 8, the averaged lifetime of **2b** decreases from 3.08 μs to 0.53 μs.

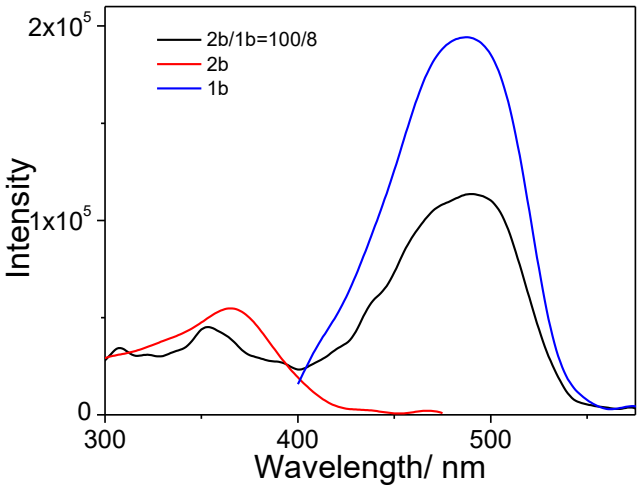

Figure S17. Excitation spectra of complex **2b**/**1b** (λ_{em} = 580nm), and the individual species.

*6. Structural characterization of **2a–b***

*6.1. Characterization of **2a***

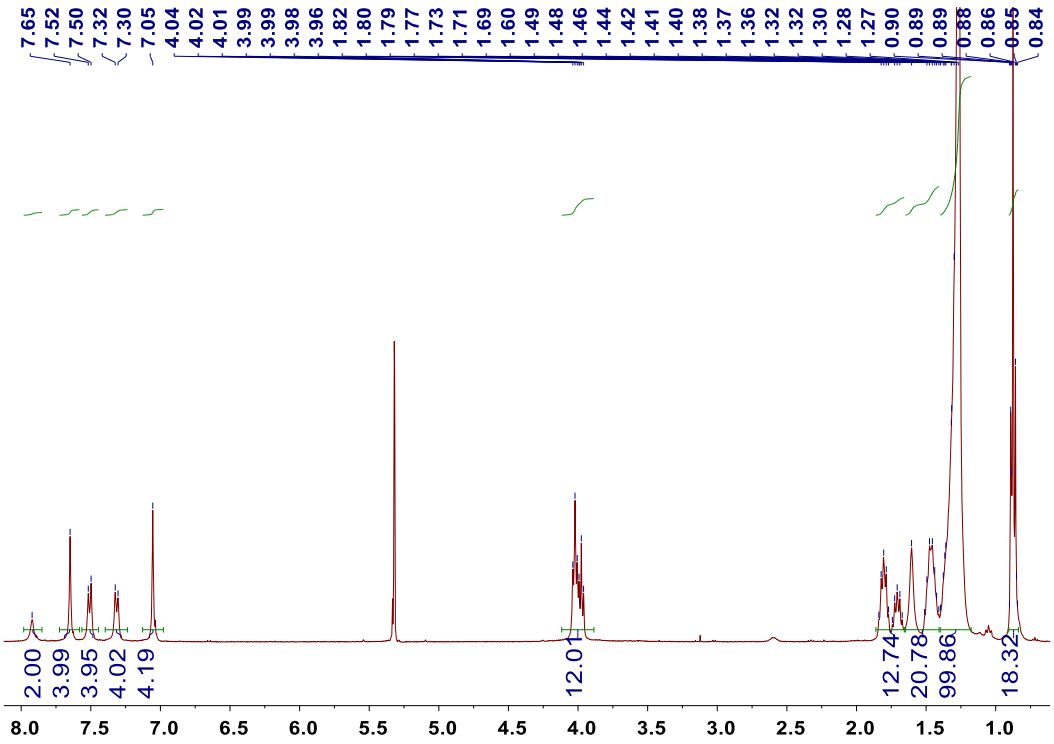

Figure S18. ^{1}H NMR spectrum (400 MHz, CD_2Cl_2, 298 K) of **2a**.

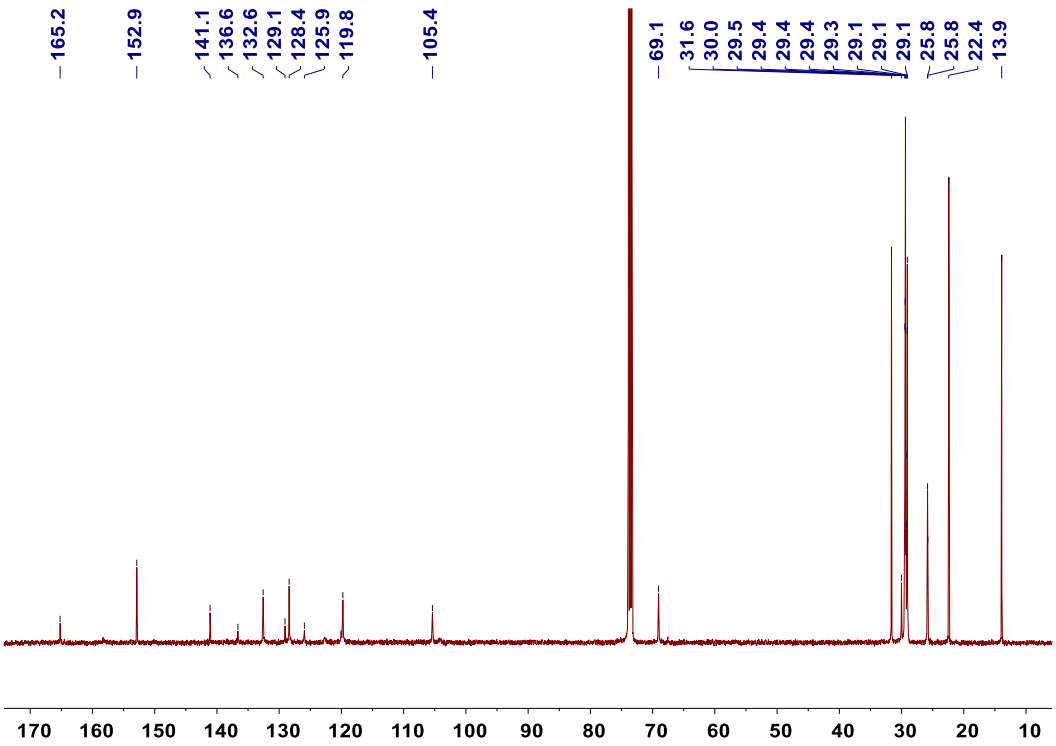

Figure S19. ^{13}C NMR spectrum (100 MHz, $C_2D_2Cl_4$, 298 K) of **2a**.

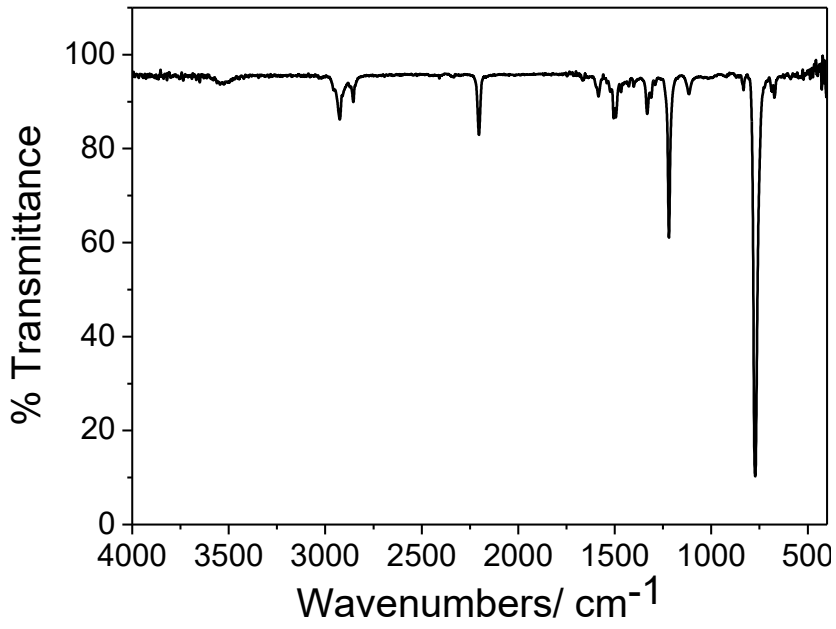

Figure S20. FT−IR spectrum of **2a**. The IR band at 2200 cm^{-1} can be assigned to the vibration peaks of C≡C unit.

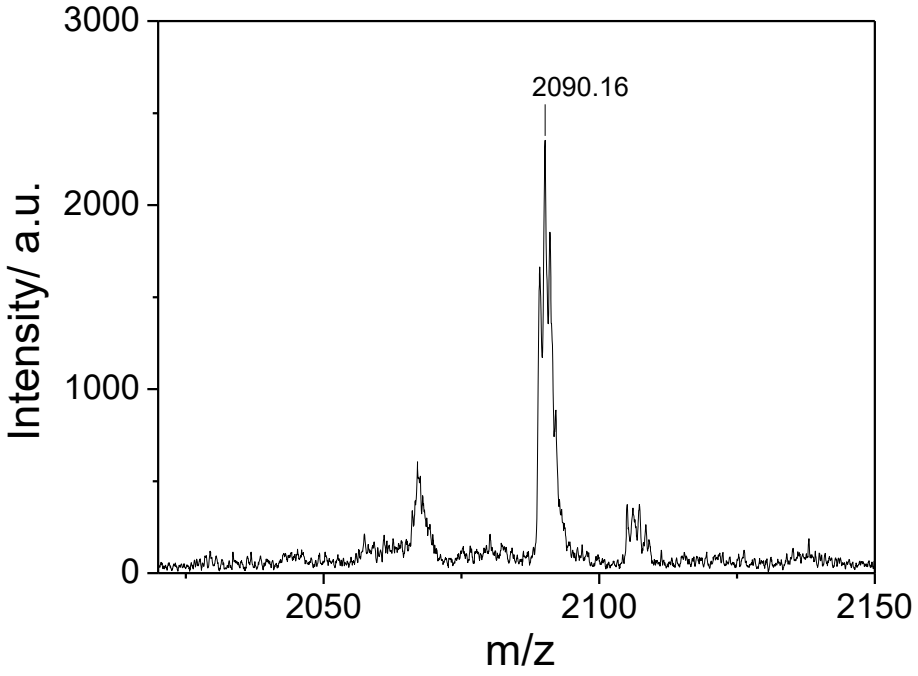

Figure S21. MALDI-TOF mass spectrum of **2a**.

*6.2. Characterization of **2b***

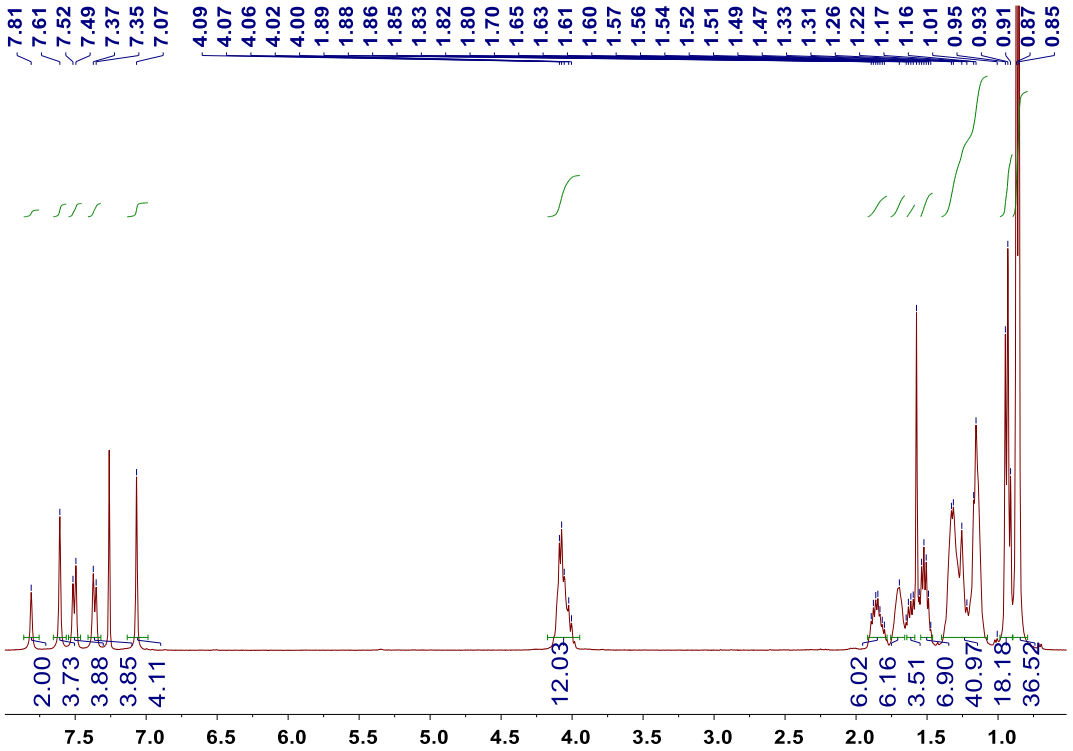

Figure S22. ^{1}H NMR spectrum (400 MHz, $CDCl_3$, 298 K) of **2b**.

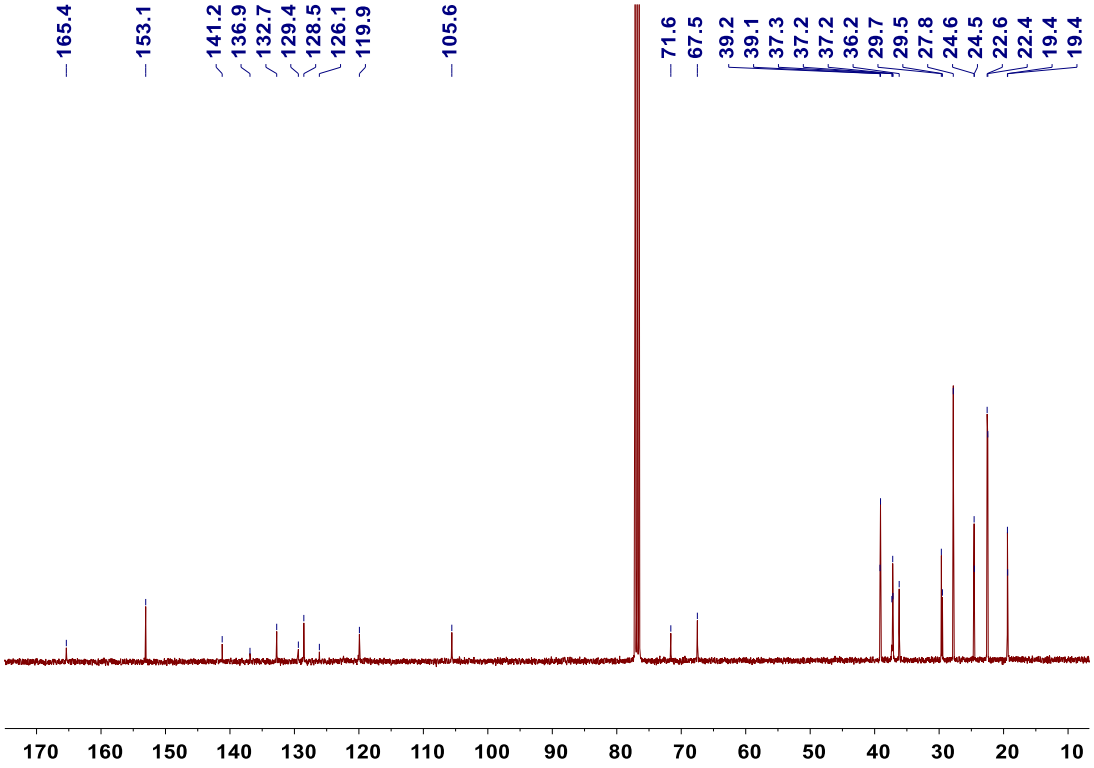

Figure S23. ^{13}C NMR spectrum (100 MHz, $CDCl_3$, 298 K) of **2b**.

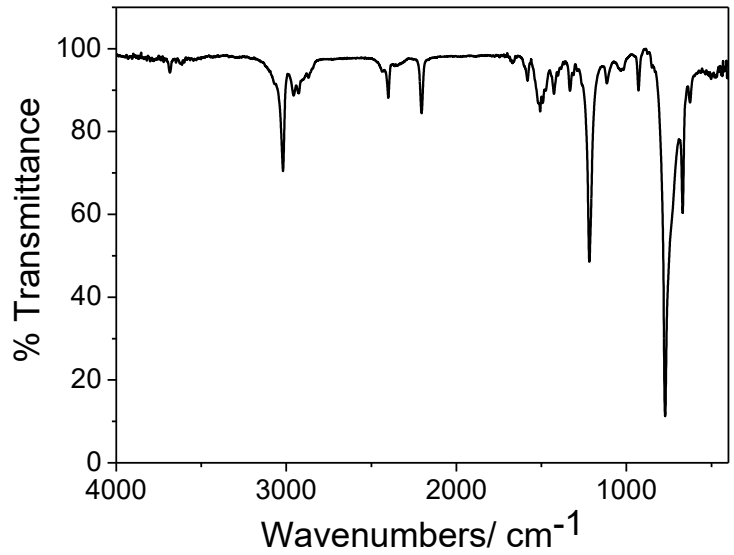

Figure S24. FT−IR spectrum of **2b**. Two IR bands are observed at 2200 cm^{-1} and 2399 cm^{-1}. They are assigned to the vibration peaks of C≡C and N≡C units, respectively.

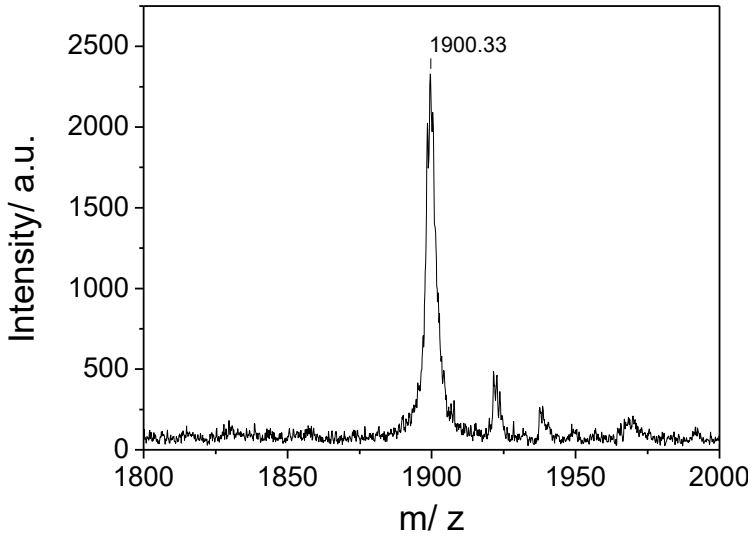

Figure S25. MALDI-TOF mass spectrum of **2b**.

REFERENCES:

S1. Z. Xu, S. Peng, Y.-Y. Wang, J.-K. Zhang, A. I. Lazar and D.-S. Guo, *Adv. Mater*., 2016, **28**, 7666.

S2. Y. Liu, S. Li, K. Li, Y. Zheng, M. Zhang, C. Cai, C. Yu, Y. Zhou and D. Yan, *Chem. Commun*., 2016, **52**, 9394.